

Molecular Electronics: Toward the Atomistic Modeling of Conductance Histograms

Published as part of *The Journal of Physical Chemistry virtual special issue "Abraham Nitzan Festschrift"*.

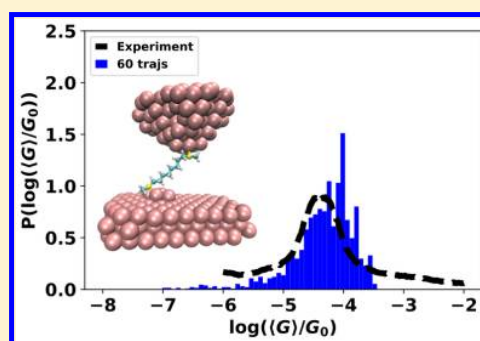
Zhi Li[†] and Ignacio Franco^{*,†,‡,§}

[†]Department of Chemistry, University of Rochester, Rochester, New York 14611, United States

[‡]Department of Physics, University of Rochester, Rochester, New York 14611, United States

Supporting Information

ABSTRACT: Reliability in molecular electronics break-junction experiments has come from statistically sampling thousands of repeat measurements. Here we discuss the computational challenges in reproducing the experimental conductance histograms and introduce a computational strategy to model molecular electronics experiments with statistics. The strategy combines classical molecular dynamics (MD) of junction formation and evolution, using a reactive force field that allows for bond-breaking and -making processes, with steady-state electronic transport computations using Green's function methods in the zero-bias limit. The strategy is illustrated using a molecular junction setup where an octanedimethylsulfide (C8SMe) connects to two gold electrodes. To attempt to reproduce the statistics encountered in experiments, we performed simulations using (1) a single MD trajectory of junction formation and evolution; (2) several MD trajectories with identical initial geometry for the electrodes; and (3) several MD trajectories each with a different geometry for the electrodes (obtained by separately crushing the electrodes and breaking the gold–gold contact). We find that these three classes of simulations can exhibit an apparent agreement with the experimental conductance histograms. Nevertheless, these simulations miss the time-averaging of the current that is inherent to the experiment. We further examined the simulated time-averaged currents for an ensemble of trajectories with crushed electrodes and found that such simulations recover the width of the experimental conductance histograms despite the additional averaging. These results highlight the challenges in connecting theory with experiment in molecular electronics and establish a hierarchy of methods that can be used to understand the factors that influence the experimental conductance histogram.



1. INTRODUCTION

Molecular electronics experiments have emerged as a powerful and versatile platform where voltages, force, and light can simultaneously be applied and used to investigate chemistry and physics at the single-molecule limit.^{1–6}

However, currently, the quantitative agreement between theoretically predicted and experimentally measured molecular conductance is typically poor,^{7–15} hindering the advancement of molecular electronics as a general platform for molecular spectroscopy and the development of molecular devices.¹⁶ This discrepancy occurs partially because of the mismatch in procedures that experiments and simulations use for capturing molecular conductance. In break-junction experiments, reproducible histograms are formed by collecting conductances from hundreds of thousands of realizations on freshly formed molecular junctions with different and uncontrolled configurations.^{1,3,17} By contrast, most computational simulations are limited to a few representative molecular and junction configurations because modeling real-time experiments and statistically sampling all experimentally relevant configurations is computationally challenging. Even approaches based on

molecular dynamics (MD) that can capture some of the conformational variability inherent to the experiments have not attempted to capture the full complexity inherent to the experiments.^{18–24} This is because these approaches often invoke fixed or implicit electrodes and do not typically capture bond-breaking and bond-making processes. In addition, approaches that have included explicit electrodes and bond-making/breaking using first-principle simulations are not able to sample all possible conformational events because of their computational cost.^{19,25–27} There have also been advances in capturing structural complexity in these experiments by sampling conformations using Monte Carlo methods.^{28–30} However, a direct comparison with experiment remains outstanding.

Such disparity between theory and experiment in molecular electronics makes it difficult to connect simulated molecular behaviors with actual experiments and develop atomistic

Received: January 11, 2019

Revised: March 27, 2019

Published: March 28, 2019

insights. Such insights are needed to understand experimental observations and, importantly, to determine the extent to which this class of experiments informs about single molecules despite the inherent averaging over realizations. Computing minimum-energy conformations and transport through higher-level electronic structure methods,³¹ while valuable, will not resolve this disparity as conductance is not dominated by minimum-energy conformations but by conformations with high conductance in the molecular ensemble.^{22,28,32–34}

In this paper, we summarize our progress in simulating the conductance histograms from atomistic simulations. Specifically, we propose a modeling strategy that takes into account explicit electrodes and captures the conformational variability during junction formation and evolution. The simulations are based on classical MD with a reactive force field³⁵ that allows modeling bond-breaking and -forming processes. These MD trajectories are coupled to computations of the zero-bias steady-state conductance using Green's function methods.³⁶ As an exemplifying case, we focus on the conductance histogram of octanedimethylsulfide (C8SMe). We choose the Au–SMe molecule–electrode contact because it exhibits simple donor–acceptor bonding features^{37–39} that allows us to focus on the statistical variations in molecular and electrode conformations, instead of the electrode–molecule binding configuration. These simulations complement efforts by Reuter et al.^{40,41} developing phenomenological models for the shape of the conductance histograms.

The structure of this paper is as follows. Section 2 describes the methods needed for modeling the dynamics and conductance of molecular junctions. Section 3 discusses a representative junction trajectory and contrasts its conductance vs elongation against experiments. In turn, section 4 discusses modeling of conductance histograms with and without time-averaging the current and how they relate to experiments. Our main results are summarized in section 5.

2. MODELING MOLECULAR JUNCTIONS WITH REACTIVE FORCE FIELD

2.1. Classical Molecular Dynamics. To capture all relevant conformational events and model the experiments with statistics, we employ classical MD simulations of junction formation and evolution using force fields. Other MD approaches^{25,42} that use first-principle-based interaction potentials are too computationally demanding for our purposes, even when employing semiempirical Hamiltonians.

In the MD, we employ the Au–S–C–H reactive force field (reaxFF)³⁵ that allows bond-breaking and -making events that are essential to understand molecular electronics break-junction experiments. This reaxFF parametrizes a bond-order-based potential to potential energy surfaces computed using density functional theory (DFT) for a variety of gold–thiol systems. The force field allows modeling of the mechanical distortion of the gold electrodes and the detachment (reattachment) of the molecule from (to) the contacts at an accuracy comparable to that of DFT but with the computational cost of a classical FF.

The MD simulations were performed using LAMMPS⁴³ in the NVT ensemble. The dynamics was propagated using a velocity-Verlet integration algorithm with a 1 fs time step and a Langevin thermostat at 300 K. At initial time, the C8SMe molecule was placed between a gold tip and a gold surface, as detailed in section 2.4. To mimic the elasticity of bulk gold, the top (or bottom) layer of the electrode was connected to a

virtual spring with a spring constant of 8 nN/m along the pulling direction⁴⁴ and rigid in perpendicular directions. The junction was thermally equilibrated for 100 fs. Subsequently, the junction was elongated by displacing the virtual spring connected to the top electrode with a constant speed of 6×10^{-7} Å/fs that guaranteed that the MD properly sampled molecular events with characteristic time scales up to ~100s of ps. The total pulling time of the junction was 50 ns with molecular snapshots recorded every 2.5 ps.

2.2. Transport Computations. Electron transport through the junction is supposed to be at steady state and well captured by the Landauer formula at all points during the elongation. The Landauer current at an applied voltage V is given by $I_{LD}(V) = \frac{e}{\pi h} \int dE [f_l(E, V) - f_r(E, V)]T(E, V)$, where f_β is the Fermi distribution of lead $\beta = l$ (left) or r (right), and $T(E, V)$ is the transmission function at energy E .

In our simulations, the conductance histograms are modeled by computing the low-bias Landauer transport for snapshots encountered during the MD. In this limit, the conductance $G = I/V = G_0 T(E_{Fermi})$ is determined by computing the transmission at the Fermi energy $T(E_{Fermi})$, where $G_0 = \frac{2e^2}{h}$ is the quantum of conductance. This quantity is computed for each snapshot encountered in the MD using Green's functions⁴⁵ in the wide-band limit and an extended Hückel Hamiltonian as implemented in Husky.³⁶ This Hamiltonian captures the essential electronic couplings and enables the simulations of several thousand conformations at a reasonable computational cost. In the method, the Fermi level E_{Fermi} of gold is an adjustable parameter chosen to be around the extended Hückel Au 6s orbital level (−10.92 eV). The precise value is chosen such that the peaks of the experimental and computational conductance histograms coincide. In the simulations below, unless noted otherwise, $E_{Fermi} \approx -11.25$ eV.

2.3. Model Electrode Geometries. In our MD simulations, we used the two sets of electrodes shown in Figure 1: (i) electrodes with well-defined predetermined

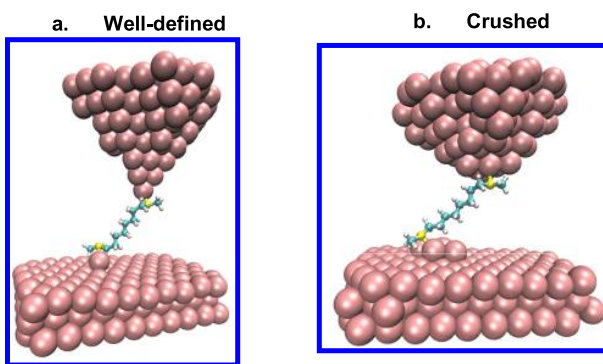


Figure 1. Different electrode and junction initial geometries employed in the simulations.

shapes and (ii) a statistical set of crushed electrodes. The electrodes with well-defined shape consist of a pyramidal gold electrode and a plate gold surface. The atomically sharp gold pyramids are seven atoms deep, while the Au(111) surfaces have three atomic layers and an extra apex atom to which the terminal S in the molecule is connected. A set of 60 different crushed electrodes is obtained by mechanically forcing electrodes into contact and subsequently pulling in analogy

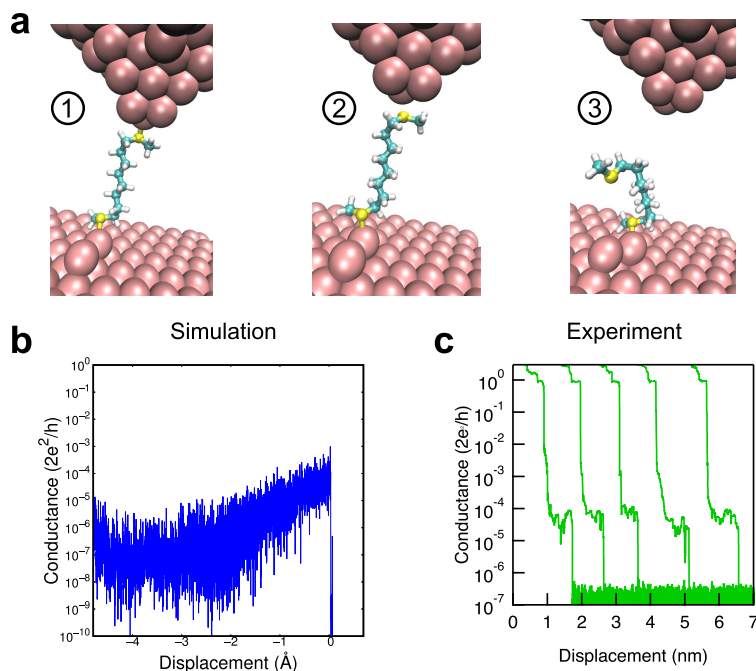


Figure 2. MD during junction formation and evolution. The plot shows (a) the bond-breaking process of a C8SMe junction under pulling and (b) simulated and (c) experimental conductance traces. The latter were kindly provided by Dr. Latha Venkataraman and Dr. Michael Inkpen.³⁷ Note that the simulated conductance trace exhibits larger fluctuation with respect to the experimental curves.

with experiments. For this, we start with the well-defined electrode geometry with the gold tip 2 Å away from the surface. We then push the tip with a constant speed $v = 6 \times 10^{-7}$ Å/fs toward the surface and displace the base of the tip for a fixed distance $\Delta > 2.0$ Å such that there is contact between the gold tip and surface. During the process, the gold atoms in the tip–surface interface rearrange. After crushing, we retract the gold tip with velocity v to separate the electrodes generating a crushed geometry. An ensemble of crushed geometries was generated by using different Δ in the 2.1–5.8 Å range.

2.4. Starting Configurations. To ensure that a molecular junction is formed in the simulations, we placed the extended molecules with its terminal S atom 2.0 Å away from the gold electrodes and at an angle with respect to the surface at the beginning of pulling. Specifically, we placed the molecule at a 45° angle with respect to the surface when using the well-defined electrodes, while a 30° angle was used in the crushed electrode case, as shown in Figure 1. Using this initial setup, the molecular junction can be elongated for 4–5 Å before junction rupture, offering a significant window into the junction evolution.

2.5. Criterion for Determining When a Junction Has Broken. To construct histograms, it is desirable to include only conductance of mechanically stable molecular junctions. As a criterion, we suppose that junctions with $\log(G/G_0) < -10.0$ correspond to broken systems and are not taken into account when constructing conductance histograms.

3. JUNCTION FORMATION AND EVOLUTION

Figure 2a,b shows MD snapshots (①–③) during the evolution of a molecular junction with a single C8SMe molecule initially bonded with gold electrodes and the resulting conductance

trace. For comparison purposes, sample experimental conductance traces for this molecule are shown in Figure 2c.

3.1. Experimental Trace. In break-junction experiments, the conductance trace starts with a gold point contact where G coincides with the quantum of conductance G_0 . When the electrodes are pulled such that the gold point contact is broken, a drop in conductance occurs, as shown in Figure 2c. After this, a conductance plateau forms near $10^{-4}G_0$, representing the conductance of a C8SMe molecular junction connecting two electrodes. As the junction breaks upon further elongation, the conductance drops to experimental resolution near $10^{-7}G_0$.

3.2. MD Strategy and Computational Trace. In the simulations, as exemplified in Figure 2a,b, a single C8SMe junction is initially bonded to two gold electrodes and the junction is subsequently mechanically extended until junction rupture. At the beginning of pulling (snapshot ①), due to compression of the molecule, the molecule adopts gauche conformations with low conductance features.²³ Upon extension, these gauche defects are eliminated and the conductance increases. During pulling, we observe that the isolated gold atoms on top of the gold surface (adatoms) move on the surface and adopt positions that can maximize the junction extension before breaking (snapshot ②). This gold adatom migration is also observed implicitly in experiments.⁴⁶ The junction is pulled until the junction bonds cannot resist the applied force, the junction breaks, and the conductance drops sharply to vacuum conductance (snapshot ③). A movie of a typical MD trajectory showing junction formation and evolution is included in the Supporting Information.⁴⁷

The simulations focus on the case in which there is just one molecule in the junction. Additional complexity can arise when there is a dense coverage of molecules in the junction, as illustrated in the simulations in refs 30, 48, and 49. The

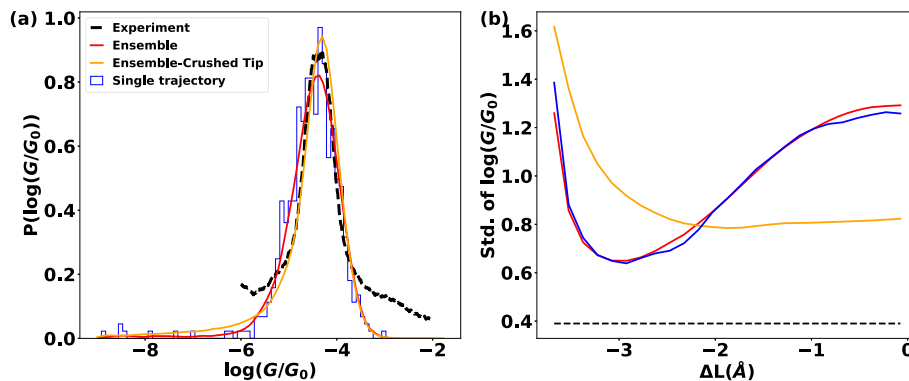


Figure 3. Simulated conductance histograms under different modeling conditions. (a) Simulated conductance distribution of the C8SMe junction constructed from a single MD trajectory (blue), many MD trajectories with identical initial electrodes (red), and with different pre-crushed initial electrode configurations (orange curve). For comparison purposes, the experimental histogram is shown in black. (b) Standard deviation of the computed conductance histograms as a function of the length before rupture ΔL taken into account in the statistics. The histograms in (a) use a distance ΔL for which the distribution is narrowest.

observed gauche defects with low conductance are in agreement with the DFT-MD simulations of an alkane dithiol molecular junction in ref 25. However, both studies contrast with the results in refs 20 and 21 that suggest that when enhanced sampling is considered the formation of gauche defects for alkane dithiols becomes less favorable due to migration of the anchor group to a side of the tip. Further, we note that the bond that breaks during the pulling using the ReaxFF is the S–Au bond. This contrasts with the DFT-MD studies in ref 50 that predict, instead, deformation of the Au electrode during pulling and breaking of the Au–Au bond.

3.3. Simulation vs Experiment. The simulated conductance vs elongation trace above captures the essential aspects of the experimental observations. Further, we note that the experimental and simulated conductance values before molecular junction rupture are comparable in magnitude and in the $10^{-4} - 10^{-5}G_0$ range. Nevertheless, there are clear differences between experimental and simulated traces. First, experiments start with a gold point contact, while simulation starts with a molecular junction. Thus, the compressed gauche conformations encountered in simulations at the beginning of pulling are not guaranteed to be encountered in experiments. Second, while the simulations show a conductance “plateau” of over 4 Å of mechanical elongation, in most of the experiments, the conductance plateau length is shorter than or around 1 Å.²⁶ Third, the simulated conductance fluctuations are larger than the experimental ones. This is particularly true for the initial stages of the pulling where the molecular junction is compressed and may undergo conformational transitions. This disparity in the simulated and experimental fluctuations in the conductance traces during elongation is because experiments report an average conductance while the simulations yield an instantaneous conductance. Because of the difference in starting point for simulated and experimental conductance vs elongation curves, we can compare only to experiments within the last ~ 1.5 Å of simulated elongation where the junctions are extended. A more detailed quantitative analysis is discussed below.

4. MODELING THE CONDUCTANCE HISTOGRAMS

We now examine the ability of different computational models of increasing complexity to reproduce the experimental conductance histogram.

4.1. Single MD Trajectory. As a first attempt to model the experimental conductance histogram, we consider a single MD trajectory with initial well-defined electrodes, as shown in Figure 1. The thermal fluctuations of the electrode and molecule during the dynamics and the conformational changes during pulling lead to a distribution of conductance values. The conductance distribution $p_L(\log(G/G_0))$ depends parametrically on junction elongation L as each L defines a different molecular ensemble. We consider the conductance distribution obtained by collecting data in the range $\Delta L = L - L_0$

$$p(\log(G/G_0)) = \frac{1}{|\Delta L|} \int_L^{L_0} p_{L'}(\log(G/G_0)) dL' \quad (1)$$

where L_0 is the elongation at which the junction breaks. The criterion employed to determine L_0 is discussed in section 2.5.

Figure 3a shows $p(\log(G/G_0))$ for a single trajectory using $|\Delta L| = 0.75$ Å (blue curve), and Figure 3b shows the influence of changing ΔL on the width of the conductance distribution. The value of ΔL chosen in Figure 3a is the one that offers a minimal width. For comparison purposes, the experimental distribution and width (black dashed line) are included in the figure. We note that in the conductance computations the Fermi energy is chosen such that the most probable conductance value in theory and experiment coincide. The simulated distributions are normalized, while the experimental conductance histogram line shape is scaled to match the maximum of the simulated distribution.

As shown, the shape and width of the simulated conductance histogram are in qualitative agreement with those from experiment. The standard deviation of $p(\log(G/G_0))$ depends strongly on ΔL ; see Figure 3b. The standard deviation increases substantially for $|\Delta L| > 0.75$ Å because as ΔL increases gauche conformations with low conductance start to play a role and broaden the histograms. In turn, for small $|\Delta L| < 0.75$ Å, while the shape of $p(\log(G/G_0))$ around its peak is approximately independent of ΔL , we note that the standard deviation also increases because low conductance conformations of partially broken junctions with $\log(G/G_0) \approx -10$ contribute appreciably to the overall standard deviation.

4.2. Multiple MD Trajectories with Identical Initial Electrodes. We now examine the influence of the stochastic nature of the MD trajectory on $p(\log(G/G_0))$. For this, we

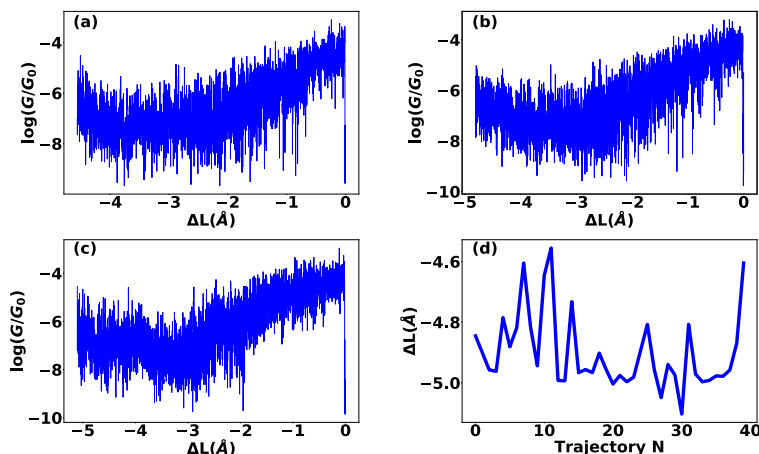


Figure 4. (a–c) Conductance traces for three MD trajectories with identical initial electrode geometries but different initial velocities and stochastic Langevin evolution. (d) Rupture length of 40 different MD trajectories.

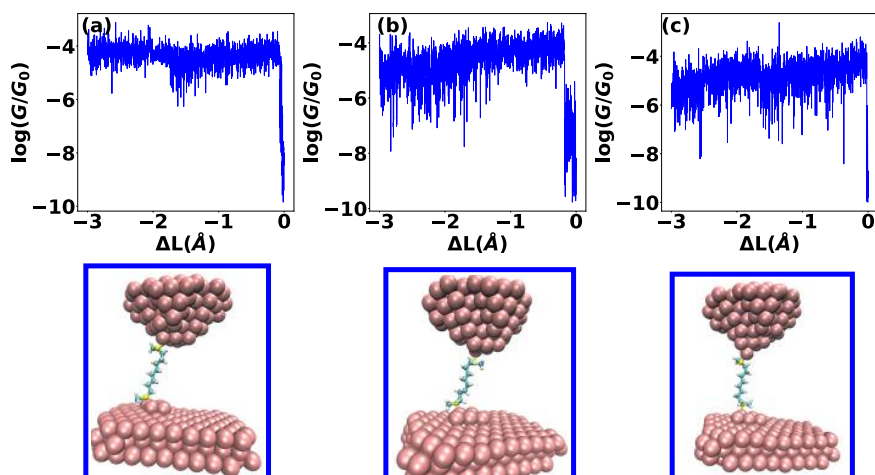


Figure 5. Individual conductance trajectories (upper panels) for three different crushed electrode geometries (lower panels).

repeated the simulations above with the same electrode and initial positions for all atoms but with different initial (random) velocities before pulling and a series of stochastic events that are encountered in the Langevin dynamics.

Figure 4 shows three representative conductance traces (a–c). While the overall shape of the trajectories is similar, they reflect different conformational dynamics and break at different points during the elongation. To explore the stochastic rupture nature of the trajectories, in Figure 4, we plot the length ΔL of each trajectory just before breaking in 40 different realizations. As can be seen, ΔL changes between trajectories even when the initial configuration is identical. Most junctions tend to rupture with $|\Delta L| \approx 4.8$ Å, but there are cases where the junction breaks with bigger and smaller ΔL . The results demonstrate that the breaking point of a junction is stochastic in nature, in agreement with the simulations in ref 30 and the theory and experiment of single-molecule force spectroscopy.^{51,52}

Figure 3a (red line) shows the resulting conductance histogram obtained by taking into account 40 trajectories with identical electrodes. The different histories of each trajectory add sources of uncertainty to the conductance histogram. We observe that including this additional source of

uncertainties does not change appreciably the shape or width of the simulated conductance distribution. Further, because the electrode and junction geometries are similar for all 40 trajectories, the dependence of the standard deviation of $p(\log(G/G_0))$ with ΔL (Figure 3b, red line) essentially coincides with that observed for a single trajectory.

4.3. Multiple MD Trajectories with Different Initial Electrodes. To investigate the effect of having different and uncontrolled electrode geometries in the simulated conductance histograms, we generated a set of 60 initial electrode geometries by crushing a pyramid gold cluster into a Au(111) surface in the MD as specified in section 2.3. This set was used to generate an ensemble of molecular junctions and collect statistics.

Figure 5 shows three representative conductance traces obtained with different precrushed electrodes. Because the crushed electrode geometries are different from each other, the conductance vs elongation curves for each one of them can be very different.

However, surprisingly, the resulting conductance histogram around $\log(G/G_0) = -4.4$ (Figure 2a, orange line) is not significantly affected by including these additional broadening contributions. This suggests that the conductance histogram in

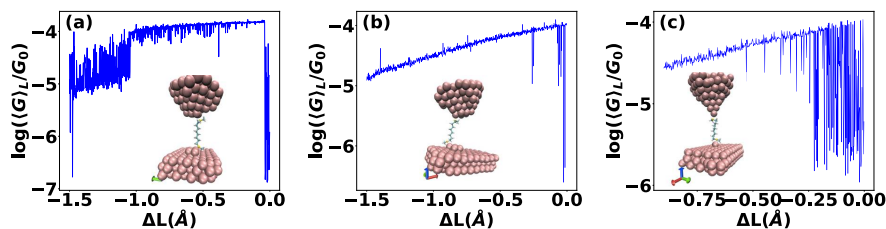


Figure 6. Average conductance $\langle G \rangle_L$ vs elongation L curves for three different initial electrode geometries. The plots illustrate the influence of time-averaging the current at each point during elongation on the conductance traces.

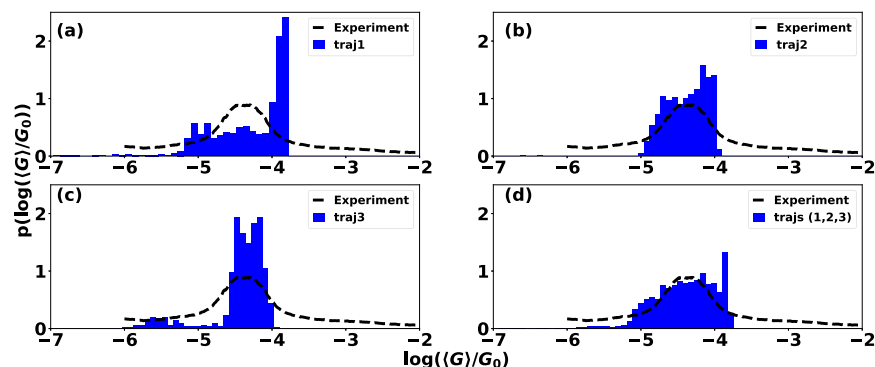


Figure 7. Conductance histogram for C8SMe constructed from the (time or ensemble) averaged $\langle G \rangle_L$ vs L . The histograms in (a–c) are constructed from the conductance traces in Figure 6. The histogram in (d) combines all available data. Experimental histograms are shown in black.

simulations for elongated junctions is dominated by thermal fluctuations and is insensitive to the precise geometry of the electrodes. This result is consistent with simulations in ref 21 that showed that the electrode shape plays a minor role in determining the conductance distribution of alkane dithiols. As shown in Figure 2b, the standard deviation of the conductance histogram in this case decreases with increasing $|\Delta L|$ for $|\Delta L| < 1.5$ Å. This is because the smaller ΔL , the more important the contributions of the conductance just after junction rupture to the conductance variance. However, as in the two previous cases, decreasing ΔL does not affect the main peak in the probability distribution. Further note that the standard deviation is larger in this case with respect to that obtained with controlled electrode geometry because the tail (i.e., $\log(G/G_0) < -6$) in the conductance distribution for the crushed electrode case is longer.

In summary, taking into account all instantaneous snapshots encountered during pulling, the shape of the simulated conductance histogram shows apparent agreement with experiment for the C8SMe molecular junction using either a single trajectory or multiple trajectories with identical or different electrodes. The implication of these numerical observations is that the distribution of conductance events is not strongly influenced by the random changes in electrode shape in and between experiments. Instead, the conductance distribution in simulations is dominated by thermal fluctuations of the molecule in the junction.

4.4. Taking into Account Time-Averages Inherent to Experiment. Simulations above yield a conductance histogram whose width and shape are in apparent agreement with experiment (recall that these results are obtained by choosing a Fermi energy such that the peaks of the experimental and simulated conductance histograms coincide). Despite this apparent coincidence between theory and experiment, there is

still a disparity in the way that the statistics are constructed in both cases. Specifically, the experiments record a current that is time-averaged, while the simulations above report the conductance of individual molecular snapshots encountered in the dynamics. We now examine the influence of time-averaging in establishing a connection between theory and experiments. The time or, equivalently, ensemble-averaged conductance distribution is

$$p(\log(\langle G \rangle_L / G_0)) = \frac{1}{|\Delta L|} \int_L^{L_0} p_L(\log(\langle G \rangle_L / G_0)) dL' \quad (2)$$

where $\langle G \rangle_L$ is the (time or ensemble) average conductance at elongation L . To do so, we performed simulations in which for each L during the pulling we determined the average conductance $\langle G \rangle_L$ for the molecular ensemble. These simulations are numerically demanding as they require a different MD simulation and subsequent transport computations for each L during the pulling. In our simulations, we collected 3.75 ns of MD per L and investigated the resulting $\langle G \rangle_L$ vs L traces.

Figure 6 shows the $\langle G \rangle_L$ vs L traces for three different electrode geometries (two crushed and one controlled). As can be seen, there are still significant conductance fluctuations despite the additional averaging that reflect different stable conformers encountered during the pulling and, for long extensions, the opening and re-forming of the molecular junctions.

The average conductance $\langle G \rangle_L$ for the three junctions is in the same conductance range of 10^{-4} – $10^{-5}G_0$ as experiments and now also shows similar conductance fluctuations (compare with Figure 2c). This contrasts with simulations in Figure 2b where conductance is not time-averaged and fluctuations are larger than the ones observed in experiments.

Figure 7 shows the conductance histograms that can be generated from these three traces. The simulated histograms are normalized, while the experimental conductance histogram line shape is scaled as Figure 3. When comparing individual histograms obtained from different trajectories (Figure 7a–c), we can see that each trajectory leads to a different conductance histogram shape. This contrasts with the observations obtained for $p(\log(G/G_0))$ without time-averaging. Even when the simulated conductance histograms do not quantitatively recover the experimental distribution of C8SMe, the width of conductance events obtained from a single $\langle G \rangle_L$ vs L trajectory is comparable to the experimental one, despite the additional averaging.

To better mimic experiments, we performed further computations of $\langle G \rangle_L$ vs L for the ensemble of 60 crushed electrodes. In these computations, we sampled L every 0.045 Å for the last 1.35 Å before junction rupture. To match with the experimental conductance histogram maximum, we choose the Fermi energy to be $E_{\text{Fermi}} = -11.1$ eV. As shown in Figure 8,

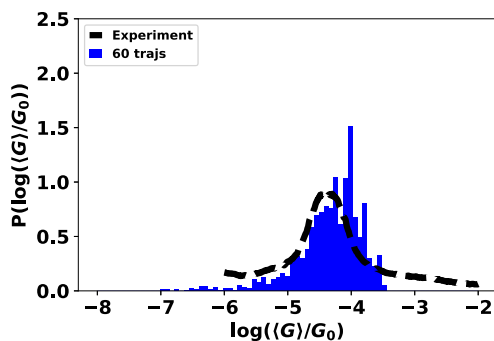


Figure 8. Conductance histogram for C8SMe constructed from time-averaged $\langle G \rangle_L$ for each point during the elongation for 60 trajectories each with a different electrode shape. Note that the Fermi energy used here is -11.1 eV.

the conductance histogram obtained with time averages and crushed electrodes shows good agreement with the experimental conductance histogram as it reproduces the width and its shape.

By comparing time-averaged conductance histograms obtained for different trajectories/electrode shapes, we find that in this case the initial conditions for the MD play an important role. This contrasts with the simulated histograms constructed with instantaneous snapshots encountered during pulling (without time-averaging) as those are dominated by thermal fluctuations. Further, we observe that when including multiple trajectories with different electrode geometries, the simulated conductance histogram can resemble the experimental one.

5. DISCUSSION

In conclusion, we simulated conductance histograms of the C8SMe molecular junction and contrasted with experimental observations. The simulations were conducted with classical MD with a reactive force field of junction formation and evolution that allows bond-breaking and -making processes and Green's function methods in the zero-bias limit for electronic transport computation. As a first attempt, we computed the conductance histograms resulting from all instantaneous snapshots encountered during the pulling. The

Fermi energy of the electrodes was chosen such that the peak of the simulated conductance distribution coincides with the experimental one. Under such conditions, we found that the shape and width of the simulated conductance histogram coincide with those of the experimental conductance histogram and for elongated junctions are not sensitive to changes in the electrode geometry or the initial conditions of the MD trajectory. While such apparent agreement is at first sight attractive, the simulations are not directly comparable to experiments because they do not take into account that experiments record a time-averaged current. To better compare with experiment, we conducted simulations for time-averaged conductance during C8SMe elongation with crushed electrodes and found that such simulations can also recover the width and shape of the experimental conductance histograms despite the additional averaging. However, to obtain such an agreement, we needed to take into account several trajectories with different initial electrode configurations.

From the analysis, to be able to match the experimental histograms using atomistic simulations, it is necessary to (1) take into account the electrodes explicitly and the bond-breaking and -forming processes; (2) statistically sample over break-junction trajectories and their conductance instead of computing the conductance of just a few representative configurations; and (3) take into account the time averages inherent to experiments. The modeling complexity reflects the many contributing factors for simulating conductance histograms. An important aspect of modeling the histogram is that junctions rupture stochastically.³⁰ The simulations showed that such stochastic rupture can lead to conductance broadening even in the case in which the junction geometry is controlled perfectly. The simulations further stress the disparity that can exist between idealized models of the junction in a minimum-energy geometry and the ensemble of conformations and junction events that determine conductance.^{22,28,32–34}

The proposed class of simulations can be used to establish a stronger connection between theory and experiment in molecular electronics and use that connection to understand the capabilities of break-junction experiments as a platform for constructing molecular devices and developing multidimensional single-molecule spectroscopies.^{22,23,33,51,53–55} Future prospects include using this class of simulations to atomistically analyze contributing factors and fundamental limits in the width of the experimental conductance histograms.

■ ASSOCIATED CONTENT

📄 Supporting Information

The Supporting Information is available free of charge on the ACS Publications website at DOI: 10.1021/acs.jpcc.9b00342.

Movie of a typical MD trajectory showing junction formation and evolution for a C8SMe junction (AVI)

■ AUTHOR INFORMATION

Corresponding Author

*E-mail: ignacio.franco@rochester.edu.

ORCID

Ignacio Franco: 0000-0002-0802-8185

Notes

The authors declare no competing financial interest.

ACKNOWLEDGMENTS

The authors thank Dr. Latha Venkataraman and Dr. Michael Inkpen for sharing the experimental data of C8SMe.

REFERENCES

- (1) Aradhya, S. V.; Venkataraman, L. Single-molecule junctions beyond electronic transport. *Nat. Nanotechnol.* **2013**, *8*, 399–410.
- (2) Ribas-Arino, J.; Marx, D. Covalent mechanochemistry: Theoretical concepts and computational tools with applications to molecular nanomechanics. *Chem. Rev.* **2012**, *112*, 5412–5487.
- (3) Xu, B.; Tao, N. J. Measurement of Single-Molecule Resistance by Repeated Formation of Molecular Junctions. *Science* **2003**, *301*, 1221–1223.
- (4) Ratner, M. A brief history of molecular electronics. *Nat. Nanotechnol.* **2013**, *8*, 378–381.
- (5) Nitzan, A.; Ratner, M. A. Electron transport in molecular wire junctions. *Science* **2003**, *300*, 1384–1389.
- (6) Hybertsen, M. S.; Venkataraman, L. Structure-Property Relationships in Atomic-Scale Junctions: Histograms and beyond. *Acc. Chem. Res.* **2016**, *49*, 452–460.
- (7) Di Ventra, M.; Pantelides, S. T.; Lang, N. D. First-Principles Calculation of Transport Properties of a Molecular Device. *Phys. Rev. Lett.* **2000**, *84*, 979–982.
- (8) Spataru, C. D.; Hybertsen, M. S.; Louie, S. G.; Millis, A. J. GW approach to Anderson model out of equilibrium: Coulomb blockade and false hysteresis in the $I - V$ characteristics. *Phys. Rev. B* **2009**, *79*, 155110.
- (9) Strange, M.; Rostgaard, C.; Häkkinen, H.; Thygesen, K. S. Self-consistent GW calculations of electronic transport in thiol- and amine-linked molecular junctions. *Phys. Rev. B* **2011**, *83*, 115108.
- (10) Baratz, A.; Baer, R. Nonmechanical Conductance Switching in a Molecular Tunnel Junction. *J. Phys. Chem. Lett.* **2012**, *3*, 498–502.
- (11) Stefanucci, G.; Kurth, S. Steady-State Density Functional Theory for Finite Bias Conductances. *Nano Lett.* **2015**, *15*, 8020–8025.
- (12) Yamada, A.; Feng, Q.; Hoskins, A.; Fenk, K. D.; Dunitz, B. D. Achieving Predictive Description of Molecular Conductance by Using a Range-Separated Hybrid Functional. *Nano Lett.* **2016**, *16*, 6092–6098.
- (13) Feng, Q.; Yamada, A.; Baer, R.; Dunitz, B. D. Deleterious Effects of Exact Exchange Functionals on Predictions of Molecular Conductance. *J. Chem. Theory Comput.* **2016**, *12*, 3431–3435.
- (14) Zhou, Q.; Yamada, A.; Feng, Q.; Hoskins, A.; Dunitz, B. D.; Lewis, K. M. Modification of Molecular Conductance by in Situ Deprotection of Thiol-Based Porphyrin. *ACS Appl. Mater. Interfaces* **2017**, *9*, 15901–15906.
- (15) Thoss, M.; Evers, F. Perspective: Theory of quantum transport in molecular junctions. *J. Chem. Phys.* **2018**, *148*, No. 030901.
- (16) Lindsay, S. M.; Ratner, M. A. Molecular transport junctions: Clearing mists. *Adv. Mater.* **2007**, *19*, 23–31.
- (17) Venkataraman, L.; Klare, J. E.; Nuckolls, C.; Hybertsen, M. S.; Steigerwald, M. L. Dependence of single-molecule junction conductance on molecular conformation. *Nature* **2006**, *442*, 904–907.
- (18) Kim, H. S.; Kim, Y.-H. Conformational and conductance fluctuations in a single-molecule junction: Multiscale computational study. *Phys. Rev. B* **2010**, *82*, No. 075412.
- (19) Pontes, R. B.; Rocha, A. R.; Sanvito, S.; Fazio, A.; da Silva, A. J. R. Ab Initio Calculations of Structural Evolution and Conductance of Benzene-1,4-dithiol on Gold Leads. *ACS Nano* **2011**, *5*, 795–804.
- (20) Paz, S. A.; Zoloff Michoff, M. E.; Negre, C. F. A.; Olmos-Asar, J. A.; Mariscal, M. M.; Sánchez, C. G.; Leiva, E. P. M. Configurational Behavior and Conductance of Alkanedithiol Molecular Wires from Accelerated Dynamics Simulations. *J. Chem. Theory Comput.* **2012**, *8*, 4539–4545.
- (21) Paz, S. A.; Michoff, M. E. Z.; Negre, C. F. A.; Olmos-Asar, J. A.; Mariscal, M. M.; Sanchez, C. G.; Leiva, E. P. M. Anchoring sites to the STM tip can explain multiple peaks in single molecule conductance histograms. *Phys. Chem. Chem. Phys.* **2013**, *15*, 1526–1531.
- (22) Pirrotta, A.; De Vico, L.; Solomon, G. C.; Franco, I. Single-molecule force-conductance spectroscopy of hydrogen-bonded complexes. *J. Chem. Phys.* **2017**, *146*, No. 092329.
- (23) Mejía, L.; Renaud, N.; Franco, I. Signatures of Conformational Dynamics and Electrode-Molecule Interactions in the Conductance Profile During Pulling of Single-Molecule Junctions. *J. Phys. Chem. Lett.* **2018**, *9*, 745–750.
- (24) Li, Z.; Tkatchenko, A.; Franco, I. Modeling nonreactive molecule–surface systems on experimentally relevant time and length scales: dynamics and conductance of polyfluorene on Au(111). *J. Phys. Chem. Lett.* **2018**, *9*, 1140–1145.
- (25) Paulsson, M.; Krag, C.; Frederiksen, T.; Brandbyge, M. Conductance of alkanedithiol single-molecule junctions: A molecular dynamics study. *Nano Lett.* **2009**, *9*, 117–121.
- (26) Quek, S. Y.; Venkataraman, L.; Choi, H. J.; Louie, S. G.; Hybertsen, M. S.; Neaton, J. B. Amine - Gold linked single-molecule circuits: Experiment and theory. *Nano Lett.* **2007**, *7*, 3477–3482.
- (27) Kamenetska, M.; Koentopp, M.; Whalley, A. C.; Park, Y. S.; Steigerwald, M. L.; Nuckolls, C.; Hybertsen, M. S.; Venkataraman, L. Formation and Evolution of Single-Molecule Junctions. *Phys. Rev. Lett.* **2009**, *102*, 126803.
- (28) French, W. R.; Iacovella, C. R.; Rungger, I.; Souza, A. M.; Sanvito, S.; Cummings, P. T. Structural origins of conductance fluctuations in gold-thiolate molecular transport junctions. *J. Phys. Chem. Lett.* **2013**, *4*, 887–891.
- (29) French, W. R.; Iacovella, C. R.; Rungger, I.; Souza, A. M.; Sanvito, S.; Cummings, P. T. Atomistic simulations of highly conductive molecular transport junctions under realistic conditions. *Nanoscale* **2013**, *5*, 3654.
- (30) Wang, H.; Leng, Y. Gold/Benzenedithiolate/Gold Molecular Junction: A Driven Dynamics Simulation on Structural Evolution and Breaking Force under Pulling. *J. Phys. Chem. C* **2015**, *119*, 15216–15223.
- (31) Yamada, A.; Feng, Q.; Zhou, Q.; Hoskins, A.; Lewis, K. M.; Dunitz, B. D. Conductance of Junctions with Acetyl-Functionalized Thiols: A First-Principles-Based Analysis. *J. Phys. Chem. C* **2017**, *121*, 10298–10304.
- (32) Berritta, M.; Manrique, D. Z.; Lambert, C. J. Interplay between quantum interference and conformational fluctuations in single-molecule break junctions. *Nanoscale* **2015**, *7*, 1096–1101.
- (33) Franco, I.; George, C. B.; Solomon, G. C.; Schatz, G. C.; Ratner, M. A. Mechanically Activated Molecular Switch through Single-Molecule Pulling. *J. Am. Chem. Soc.* **2011**, *133*, 2242–2249.
- (34) Ding, W.; Negre, C. F. A.; Vogt, L.; Batista, V. S. High-Conductance Conformers in Histograms of Single-Molecule Current–Voltage Characteristics. *J. Phys. Chem. C* **2014**, *118*, 8316–8321.
- (35) Järvi, T. T.; van Duin, A. C. T.; Nordlund, K.; Goddard, W. A. Development of Interatomic ReaxFF Potentials for Au–S–C–H Systems. *J. Phys. Chem. A* **2011**, *115*, 10315–10322.
- (36) Frisenda, R.; Janssen, V. A. E. C.; Grozema, F. C.; van der Zant, H. S. J.; Renaud, N. Mechanically controlled quantum interference in individual π -stacked dimers. *Nat. Chem.* **2016**, *8*, 1099–1104.
- (37) Park, Y. S.; Whalley, A. C.; Kamenetska, M.; Steigerwald, M. L.; Hybertsen, M. S.; Nuckolls, C.; Venkataraman, L. Contact chemistry and single-molecule conductance: A comparison of phosphines, methyl sulfides, and amines. *J. Am. Chem. Soc.* **2007**, *129*, 15768–15769.
- (38) Frei, M.; Aradhya, S. V.; Hybertsen, M. S.; Venkataraman, L. Linker dependent bond rupture force measurements in single-molecule junctions. *J. Am. Chem. Soc.* **2012**, *134*, 4003–4006.
- (39) Aradhya, S. V.; Nielsen, A.; Hybertsen, M. S.; Venkataraman, L. Quantitative bond energetics in atomic-scale junctions. *ACS Nano* **2014**, *8*, 7522–7530.
- (40) Williams, P. D.; Reuter, M. G. Level alignments and coupling strengths in conductance histograms: The information content of a single channel peak. *J. Phys. Chem. C* **2013**, *117*, 5937–5942.

- (41) Quan, R.; Pitler, C. S.; Ratner, M. A.; Reuter, M. G. Quantitative Interpretations of Break Junction Conductance Histograms in Molecular Electron Transport. *ACS Nano* **2015**, *9*, 7704–7713.
- (42) Soler, J. M.; Artacho, E.; Gale, J. D.; García, A.; Junquera, J.; Ordejón, P.; Sánchez-Portal, D. The SIESTA method for ab initio order-*N* materials simulation. *J. Phys.: Condens. Matter* **2002**, *14*, 2745.
- (43) Plimpton, S. Fast Parallel Algorithms for Short-Range Molecular Dynamics. *J. Comput. Phys.* **1995**, *117*, 1–19.
- (44) Rascón-Ramos, H.; Artés, J. M.; Li, Y.; Hihath, J. Binding configurations and intramolecular strain in single-molecule devices. *Nat. Mater.* **2015**, *14*, 517–522.
- (45) Datta, S. *Quantum transport: Atom to transistor*; Cambridge University Press: New York, 2005.
- (46) Maksymovych, P.; Sorescu, D. C.; Yates, J. T. Gold-atom-mediated bonding in self-assembled short-chain alkanethiolate species on the Au(111) surface. *Phys. Rev. Lett.* **2006**, *97*, 1–4.
- (47) See the [Supporting Information](#) for a movie of a typical C8SMe junction MD trajectory showing junction formation and evolution.
- (48) Pu, Q.; Leng, Y.; Zhao, X.; Cummings, P. T. Molecular Simulation Studies on the Elongation of Gold Nanowires in Benzenedithiol. *J. Phys. Chem. C* **2010**, *114*, 10365–10372.
- (49) French, W. R.; Iacovella, C. R.; Cummings, P. T. Large-scale atomistic simulations of environmental effects on the formation and properties of molecular junctions. *ACS Nano* **2012**, *6*, 2779–2789.
- (50) Krüger, D.; Fuchs, H.; Rousseau, R.; Marx, D.; Parrinello, M. Pulling Monatomic Gold Wires with Single Molecules: An Ab Initio Simulation. *Phys. Rev. Lett.* **2002**, *89*, 186402.
- (51) Franco, I.; Schatz, G. C.; Ratner, M. A. Single-molecule pulling and the folding of donor-acceptor oligorotaxanes: Phenomenology and interpretation. *J. Chem. Phys.* **2009**, *131*, 124902.
- (52) Dudko, O. K.; Hummer, G.; Szabo, A. Theory, analysis, and interpretation of single-molecule force spectroscopy experiments. *Proc. Natl. Acad. Sci. U. S. A.* **2008**, *105*, 15755.
- (53) Koch, M.; Li, Z.; Nacci, C.; Kumagai, T.; Franco, I.; Grill, L. How Structural Defects Affect the Mechanical and Electrical Properties of Single Molecular Wires. *Phys. Rev. Lett.* **2018**, *121*, No. 047701.
- (54) Pirrotta, A.; Solomon, G. C.; Franco, I. Hydrogen Bonding in Tight Environments: Simulated Force Spectroscopy of Nanoconfined Hydrogen-Bonded Complexes. *J. Phys. Chem. C* **2016**, *120*, 19470–19478.
- (55) Pirrotta, A.; Solomon, G. C.; Franco, I.; Troisi, A. Excitonic Coupling Modulated by Mechanical Stimuli. *J. Phys. Chem. Lett.* **2017**, *8*, 4326–4332.